Motagh, M., Bahroudi, A., Haghshenas Haghighi, M., Samsonov, S., Fielding, E., Wetzel, H.-U. (2015): The 18 August 2014 Mw 6.2 Mormori, Iran, Earthquake: A Thin-Skinned Faulting in the Zagros Mountain Inferred from InSAR Measurements. - *Seismological Research Letters*, *86*, 3, p. 775-782.

DOI: http://doi.org/10.1785/0220140222

The 18 August 2014 M_w 6.2 Mormori, Iran, Earthquake: A Thin-Skinned Faulting in the Zagros Mountain Inferred from InSAR Measurements

by Mahdi Motagh, Abbas Bahroudi, Mahmud Haghshenas Haghighi, Sergey Samsonov, Eric Fielding, and Hans-Ulrich Wetzel

Online Material: Figures of interferograms, posteriori probability distribution of fault parameters, tradeoff curve, checkerboard test and modeling results for entire area, and tables of boundaries used in the inversion and of digital slip distribution.

INTRODUCTION

Studies of fault geometry and slip distribution associated with large earthquakes are important to improve our understanding of how continental lithosphere behaves physically in response to plate tectonic motions. The Zagros mountain fold-and-thrust belt in southwestern Iran is one of the largest and most active belts on our planet with continuous seismicity. This northwest–southeast-trending belt extends in southwestern Iran within the Alpine–Himalayan orogenic chain, accommodating approximately 10 mm/yr of north–south shortening between Arabia and Eurasia (Nilforoushan *et al.*, 2003; Tatar *et al.*, 2004; Vernant *et al.*, 2004). Earthquakes with moderate magnitudes of 5.5–6 m_b are common in the ~250–350 km wide zone along the Zagros fold-and-thrust belt (Jackson, 1980a; Berberian, 1995). Although, most of these earthquakes within the belt are not accurately located by teleseismic data (Jackson and Fitch, 1981; Ni and Barazangi, 1986), studies suggest that the seismicity has been restricted to a depth of less than 40 km (Maggi *et al.*, 2000).

Much work has been done in the past to improve our understanding of the shortening mechanism in the Zagros (Koyi *et al.*, 2000; Tatar *et al.*, 2004; Yamini-Fard *et al.*, 2007; Authemayou *et al.*, 2009; Oveisi *et al.*, 2009). Both thick-skinned deformation (Jackson, 1980b; Berberian, 1995) and thin-skinned deformation (Hessami *et al.*, 2006; Walpersdorf *et al.*, 2006) models have been proposed for geodynamic evolution of Zagros orogeny; in the former model, the shortening is accommodated by reverse basement faulting that is separated from shallow sedimentary rocks by the infra-Cambrian Hormuz salt sequence, and, in the latter model, active folding of the shallow sediments is the main deformation mechanism. The rate of shortening in the basement is estimated to be an order of magnitude lower than that in the sedimentary cover (Sherkati *et al.*, 2006). However, due to lack of a dense seismic and geodetic network, it is difficult to precisely assess deformation partitioning in detail and to evaluate to what extent the folding of the thick sedimentary cover of 5–15 km is decoupled from the basement faulting at depth in different segments.

In this article, we investigate source parameters and the fault-slip distribution of the 2014 M_w 6.2 Mormori, Iran, earthquake using interferometric observations. Centered at 32.71° N and 47.64° E, the event occurred on 18 August 2014 at 2:32 UTC, near Mormori, a small town in Ilam province of southwest Iran (http://irsc.ut.ac.ir; last accessed April 2015). The mainshock was preceded by two foreshocks of magnitudes M_w 4.5 and 4.6 on 17 August 2014, which triggered an evacuation warning in the area; as a result, the earthquake caused no fatalities, although 250 people were injured and more than 10,000 became homeless (http://www.iaee.or.jp; last accessed April 2015). The M_w 6.2 mainshock on 18 August was followed by a vigorous aftershock sequence with seven $M_w > 5$ events up to 25 October 2014, including an M_w 5.9 event on 18 August that makes the earthquake sequence almost a doublet. Focal plane solutions from the Global Centroid Moment Tensor (Global CMT) and Iranian Seismological Center (ISC) catalogs (http://irsc.ut.ac.ir; last accessed April 2015) show mainly reverse faulting for both events.

The main tectonic setting of the western Zagros is characterized from northeast to southwest (Fig. 1) by right-lateral strike-slip faulting along the main recent fault (MRF) and thrust faulting along several basement thrusts including main Zagros reverse fault (MZRF), high Zagros fault (HZF), Dezful embayment fault (DEF), mountain front fault (MFF), and Zagros foredeep fault (ZFF). The mainshock and early aftershocks of the 2014 Mormori event lie on the Dezful embayment to the south of the MFF fault (Fig. 1), which is an unexposed high-

doi: 10.1785/0220140222

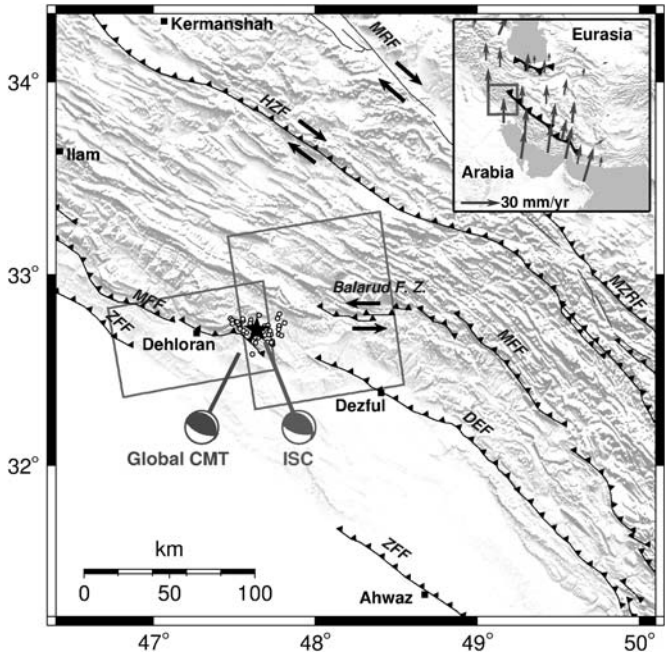

▲ **Figure 1.** Shaded relief map and main tectonic setting of the study area, modified from the map of major active faults in Iran (Hessami *et al.*, 2003). Active faults aer shown as black lines: MRF, main recent fault; MZRF, main Zagros reverse fault; HZF, high Zagros fault; DEF, Dezful embayment fault; MFF, Mountain front fault; and ZFF, Zagros foredeep fault. The black star and white dots are the epicenter location and aftershocks ($M_w \geq 4$, depth < 20 km for the first 10 days after the mainshock), respectively; the data were taken from the Iranian Seismological Center (ISC) catalog. The focal mechanisms are from the ISC and Global Centroid Moment Tensor (CMT) catalogs. Gray rectangular outlines indicate the coverage of the RADARSAT-2 images. The inset shows the main tectonic settings of Iran, with Global Positioning system velocities from (Vernant *et al.*, 2004). The box in the inset map is the study area.

relief structure in the Zagros showing an irregular pattern in map view and involving several asymmetric folds (Oveisi *et al.*, 2009). At latitude of 32.9° N and longitude 47.5° E the MFF is offset by about 130 km along the left-lateral fault zone of Balarud (Berberian, 1995; Bahroudi and Koyi, 2003). Using interferometric measurements, we obtain source parameters of the 2014 Mormori earthquake and analyze it against geological data and seismic cross sections to examine whether the earthquake is related to the fold activation in sedimentary cover or to deep basement faulting in the Zagros.

DATA AND METHODOLOGY

Two ascending RADARSAT-2 interferograms are used in this study. The first interferogram is computed from Wide Multi-Look Fine 3 (MF3W, incidence angle 43°, azimuth 350°) images acquired on 2 May 2013 and 25 August 2014 with the perpendicular baseline of 26 m. The second interferogram is computed from two Standard 8 (S8, incidence angle 50°, azimuth 351°) images acquired on 2 December 2012 and 11 September 2014 with the perpendicular baseline of 85 m. The gray boxes in Figure 1 illustrate the outline of the areas covered by the RADARSAT-2 images. The interferometric processing is performed with the GAMMA software (Wegmuller and Werner, 1997), consisting of slave-to-master images coregistration and resampling, interferogram computation while applying multilooking (i.e., spatial averaging, 7×7 for MF3W and 2×10 for S8), topographic phase removal using the 30 m ASTER DEM, the adaptive filtering with filtering function based on local fringe spectrum (Goldstein and Werner, 1998), phase unwrapping using the minimum cost flow algorithm (Costantini, 1998), and geocoding to a 20 m grid.

The unwrapped results are then inverted using dislocations in homogenous elastic half-space (Okada, 1985). The inversion is done in two steps: first we invert Interferometric Synthetic Aperture Radar (InSAR) observations using the Bayesian inversion (Fukuda and Johnson, 2008; Faegh-Lashgary *et al.*, 2012) to obtain the most probable fault geometry parameters of a single uniform-slip dislocation. There is a well-known tradeoff between the amount of slip and width of the rupture when constructing a fault model using geodetic data (Atzori *et al.*, 2009; Atzori and Antonioli, 2011), and there are also tradeoffs between the rake and amount of slip when only one InSAR line-of-sight (LOS) measurement is used. The two ascending RADARSAT-2 interferograms have LOS vectors that only differ by 7°. The moment tensor solutions of the mainshock and early aftershocks suggest that the 2014 earthquake sequence is dominated mainly by thrust faulting (ISC catalog). We assume that such faulting occurred on the same fault plane and therefore first invert the InSAR data by fixing the strike-slip component to be zero then solve for the remaining parameters.

Second, having obtained the most probable fault geometry parameters, the InSAR measurements d are inverted for a distributed slip distribution s by minimizing the following function (Harris and Segall, 1987):

$$\phi = \|Gs - d\|^2 + \alpha^2 \|Hs\|, \quad (1)$$

in which G is the dislocation Green's function, H is the finite-difference approximation of the Laplacian operator, and α is the smoothing factor that controls the tradeoff between data misfit and model roughness. To obtain the slip model with regularization, we extend the fault width along the dip direction, discretize the rectangular fault plane into a grid of 1 km × 1 km patches, and invert for variable dip slip with $\alpha = 0.05$ as determined by the tradeoff curve (see Ⓔ Fig. S3, available in the electronic supplement to this article). The constrained least-squares optimization problem in equation (1) is solved using an iterative algorithm called steepest descent method (Wang *et al.*, 2013).

RESULTS

Despite the long (> 1 year) temporal baselines, the coherence is good in both interferograms due to lack of vegetation and dry climate in this region, resulting in reliable phase unwrap-

ping. However, both interferograms show fringe structures mimicking topography in many parts, indicating artifact contribution due to changes in atmospheric water vapor (especially the vertical gradient) between Synthetic Aperture Radar (SAR) data acquisitions (Li *et al.*, 2005). To mitigate this effect, together with any artifact fringes resulting from orbital errors, we consider a bilinear ramp plus linear height dependence model $z = ax + by + cH + d$, in which x, y, and H are east, north, and height of each pixel, respectively, in the geocoded interferogram, and z is displacement. We fit this model to the unwrapped interferograms, assuming that the far-field displacement is zero (Wen *et al.*, 2013). The potential deformation area around the epicenter is masked out before estimating the coefficients of a, b, c, and d.

The corrected interferograms show improvement in the results with most of the residual turbulent signals related to topography have been removed. Figure 2a,d shows a close-up view of the two interferograms after atmospheric correction (see Ⓔ Fig. S1 for the original view of the interferogram). The root mean square (rms) of noise in 2013.05.02–2014.08.25 and 2012.12.02–2014.09.11 interferograms is reduced from 1.9 and 1.7 to 1.3 and 1 cm, respectively. Clear fringe lobes around the epicenter area are now observable (Fig. 2a,d), showing LOS displacement toward the satellite (uplift and westward motion).

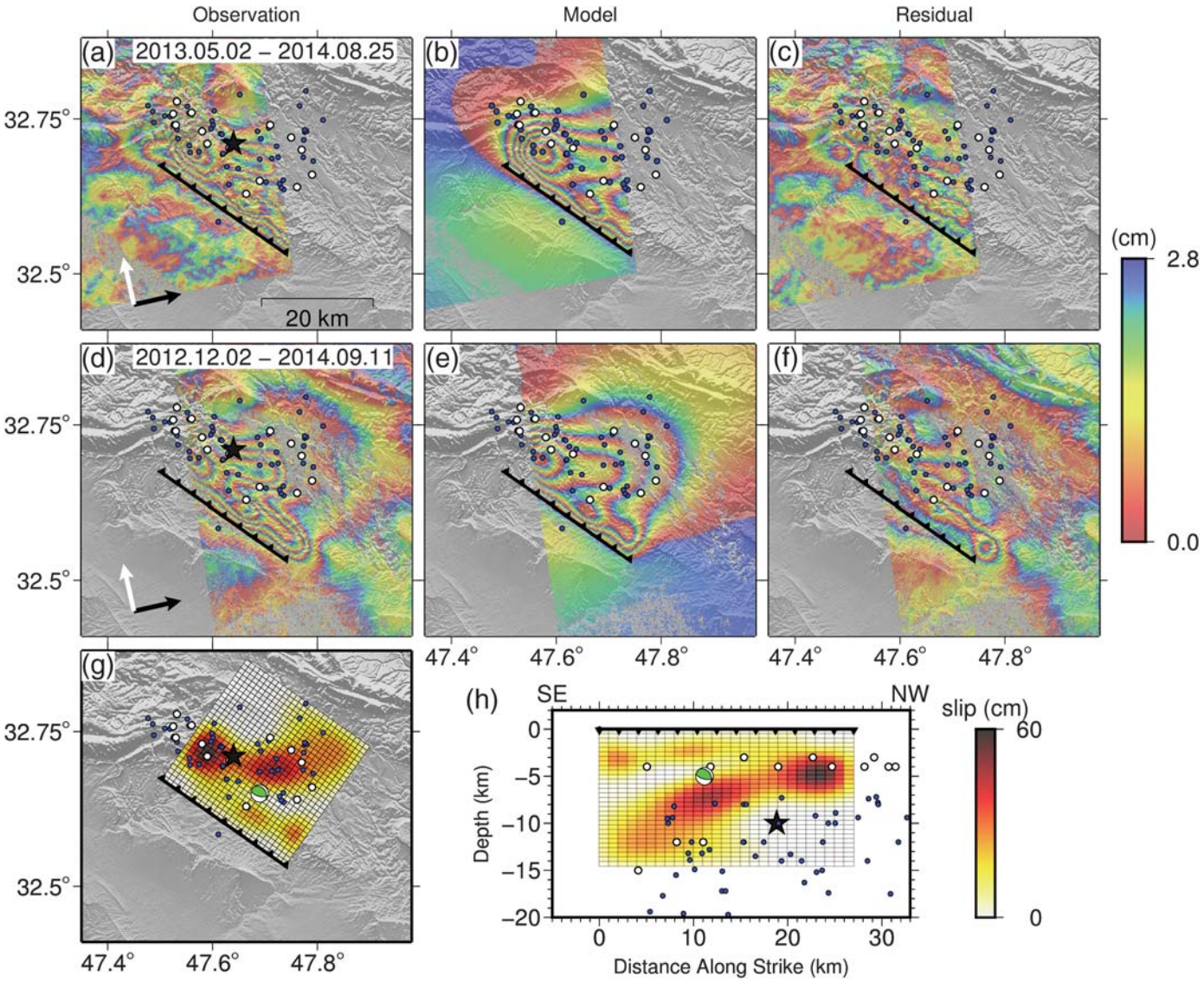

▲ **Figure 2.** (a–f) A close up view of interferograms, models, and (g–h) residuals based upon the slip distribution model. The interferograms in (a) and (d) have been unwrapped and rewrapped again with each fringe representing 2.8 cm of line-of-sight (LOS) displacement from ground to satellite. Black line, up-dip projection of the modeled fault plane to the surface; black star, mainshock epicenter; blue circles, aftershocks for the first 10 days taken from the ISC catalog; white circles, aftershocks with known focal mechanism solution from the ISC catalog; white arrow, azimuth direction; and black arrow, LOS direction. (g) Map view of the coseismic slip distribution. (h) Cross-section view of the slip distribution. Green beach ball in (g) and (h) corresponds to centroid location and depth, respectively, taken from ISC.

The uplifted region extending south from the epicenter covers an area of about 31 km northwest–southeast and 17 km northeast–southwest. The maximum LOS uplift is about 18 cm. We stress that in this region the topography variation is not as high as in other parts to the north (Fig. 3b), and therefore phase contribution to the interferometric phase due to tropospheric stratification is not as severe as in other parts of the interferograms. The similarity between deformation areas in both corrected interferograms suggests that most of the remaining signals are mainly due to the earthquakes, with some contribution from heterogeneous water vapor distribution that was not modeled above.

The fault plane for the 18 August 2014 earthquake inferred from the Bayesian inversion of InSAR data has a length and width of about 27 and 19 km, respectively. It strikes ~304° with a dip angle of ~29° toward the northeast (see Ⓔ Fig. S2 for the *a posteriori* probability distribution function of fault parameters). Figures 2g,h illustrates the final slip distribution in map and cross-section view, respectively. Our result identifies two major patches of slip release: a northern patch at a depth close to 5 km with a peak slip of 60 cm and a southern patch beneath the centroid depth with a peak slip of about 45 cm. The centroid of the southern patch is 2–3 km deeper than the northern patch. A checkerboard test was performed (see Ⓔ Fig. S4) and showed the slip is the shallow part of the fault (<10 km) that is well resolvable in the inversion, in particular for the northern patch. The fault dislocation does not reach to the surface with motion constrained between 3 and 10 km. The total geodetic moment is 3.518×10^{18} N·m (M_w 6.30) using a crustal shear modulus of 30 GPa. The geodetic moment that we derive from the slip model (Fig. 2h) is slightly (18%) larger than the cumulative seismic moment release from the M_w 6.2 mainshock ($M_0 = 2.14 \times 10^{18}$) and its largest M_w 5.9 aftershock ($M_0 = 7.5 \times 10^{17}$), suggesting that the seismic slip from individual aftershocks contributed to the coseismic deformation field recorded by InSAR observations. Table S2 contains the slip model and can be downloaded from the electronic supplement.

As seen in Figure 2b,c,e,f, the pattern of LOS uplift south of the epicenter is well reproduced by the slip model in Figure 2g. The rms misfit between the observations and model prediction in the far field (>30 km from the fault trace), of the order of 1 cm for both interferograms, is representative of the approximate level of atmospheric noise in each image (see Ⓔ Fig. S5). The residuals seen in the near-fault area (Fig. 2c,f) probably reflect the influence of local fault geometry on the displacement field and/or inelastic deformation induced by aftershock sequence (Wang *et al.*, 2010).

DISCUSSION

Figure 3 illustrates the up-dip projection of the 2014 model fault plane on a Landsat 7 image of the area. The Mormori earthquake sequence occurred in the Dezful embayment, which is a structural depression in the central part of the Zagros fold-and-thrust belt. The MFF as a major structural step forms the northeast boundary to the Dezful embayment (Fig. 1). Previous studies attributed MFF to the rigid Precambrian basement of the belt that is exposed in the western part of the Arabian shield (Falcon, 1967; Husseini, 1988; Konert *et al.*, 2001); however, the role of the basement fabrics and their seismicity are still not well known. For some cases in the eastern part of the Iranian continental plateau, the causal relationship between blind-reverse faulting and surface folding has been well documented (Walker *et al.*, 2003; Walker, 2006), but this is not the case for the Zagros mountains, in which the thick sedimentary cover is decoupled from the old rigid basement by the extensive Hormuz salt. The sedimentary cover of the Zagros mountains is 5–15 km thick, which includes platform carbonates, marls, sandstone, and shale with some evaporate horizons as decollements in different levels (Bahroudi and Koyi, 2003; Sherkati *et al.*, 2006).

The Dezful embayment contains several anticlinal structures hosting super-giant hydrocarbon fields, formed by different mechanisms (fault-related and detachment folding). In some reflective seismic profiles, compressional low and high-angle faults can be detected clearly in the southwest limb of the anticlinal structures. These faults die up-section or sole out in evaporitic units of the Gachsaran formation.

The horizontal location of the InSAR-derived fault plane for the 2014 event is close to the northwest–southeast-trending Dalpari anticline, located within the western part of the Dezful embayment in the Lorestan province of southwest Iran, about 70 km northwest of Dezful and 40 km east of Dehloran (Figs. 1, 3). This structure is a small anticline, 13 km long and 5 km wide. Toward the sinistral strike-slip fault zone of Balarud, the axial trace of the Dalpari anticline is deflected to the north and probably resulted from offset of the Balarud fault. Bahroudi and Koyi (2003) suggested that the map-view observed offset of the MFF along the Balarud fault may not be entirely caused by the strike-slip movement along reactivated basement faults, but from faulting within the sedimentary cover overlying the rigid basement.

The InSAR-derived dip angle of 29° NE implies a low-angle thrust faulting during the 2014 sequence, assuming all the slip of the mainshock and aftershocks occurred on the same planar fault. The CMT solution using a local seismic network (ISC catalog) gives two nodal planes for the mainshock, one (NP1) dipping 63° SW with the strike of 104° and rake of 72° and another (NP2) dipping 32° NE with the strike of 320° and rake of 121°. The focal solutions reported by the Global CMT catalog and U.S Geological Survey/National Earthquake Information Center (USGS/NEIC) provide similar mechanisms for NP1 and NP2 (Table 1). Previous studies suggest the existence of both north-dipping and south-dipping active thrust in the Zagros (Nissen *et al.*, 2007, 2010; Roustaei *et al.*, 2010). Our fault model for the 2014 Mormori earthquake strongly favors a northeast-dipping NP2 plane in seismic observations. The northeast dip is also consistent with the geologic cross section from the National Iranian Oil Company (Fig. 3c).

The inversion of InSAR data suggests the main faulting associated with the 2014 sequence is restricted to a depth between 3 and 10 km, which is in agreement with the shallow centroid depth estimated from local seismic observations (Fig. 3c) and USGS/NEIC body waves inversion (Table 1).

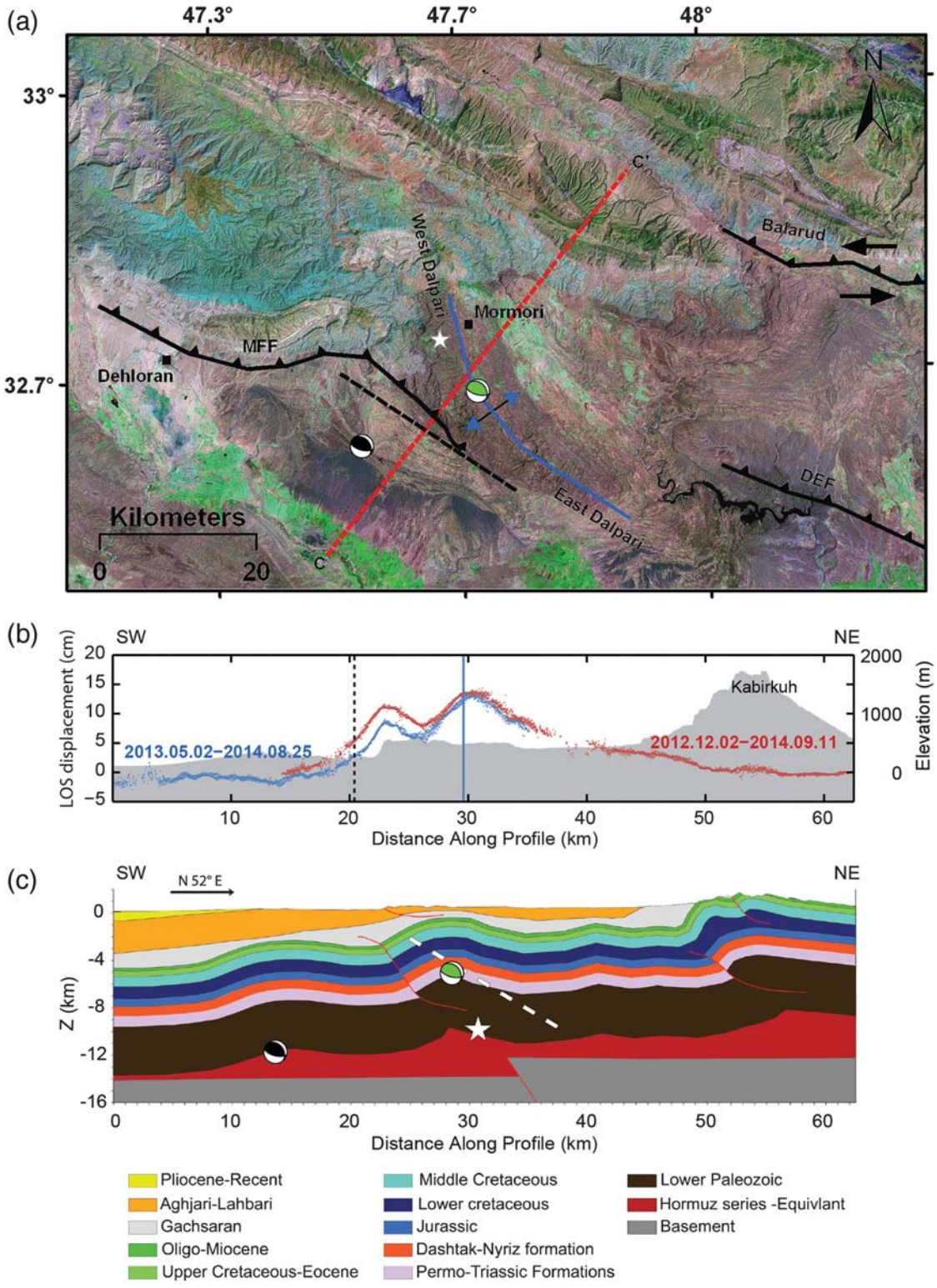

▲ **Figure 3.** (a) The Landsat 7 image (RGB composite bands 7,4,2) of the Mormori region. The dashed black line shows the surface projection of the 2014 fault plane derived from InSAR observations. (b) Profile of the LOS deformation and topography along CC′ in (a). The black dashed line indicates the intersection of the profile with the up-dip projection of the fault plane, and the blue line shows the intersection with the Dalpari anticline. (c) Simplified seismic profile along CC′, modified based on the geological map from National Iranian Oil Company (NIOC) with red lines showing thrust faults (Setudehnia and OB-Perry, 1967; Sahabi and Macleod, 1969). The white dashed line shows the main fault zone of the 2014 Mormori earthquake at depth. The black and green focal mechanisms correspond to the centroid location taken from the Global Centroid Moment Tensor (CMT) (http://www.globalcmt.org, last accessed April 2015; event ID: 201408180232A) and the ISC catalogs, respectively. The white star is the ISC hypocenter location.

Table 1
Focal Mechanism Solution of the 2014 Mormori Earthquake from Catalogs of USGS/NEIC, Global CMT, and ISC

Solution	Magnitude	Depth (km)	Np1 (Strike, Dip, Rake)	Np2 (Strike, Dip, Rake)
USGS/NEIC	6.2	4.0	121°, 79°, 89°	308°, 12°, 97°
Global CMT	6.2	12.0	114°, 65°, 80°	317°, 27°, 111°
ISC	6.2	5.0	104°, 63°, 72°	320°, 32°, 121°

USGS/NEIC, U.S Geological Survey/National Earthquake Information Center; Global CMT, Global Centroid Moment Tensor; ISC, Iranian Seismological Center.

The Global CMT point-source inversion using long-period body and surface waves suggests a deeper source of about 12 km (black beach ball in Fig. 3c). Therefore, from InSAR observations, we can infer that the faulting has been restricted to the sedimentary cover. This together with the other fault parameters explained above, implies that the earthquake can be attributed to the active fault-related folding of the Dalpari anticline at depth.

We used a homogenous half-space in order to calculate the Green's functions and invert the InSAR data for slip distribution. Several studies have addressed the importance of vertical crustal layering and the effect that this imparts on the coseismic deformation field (Wang *et al.*, 2003; Amoruso *et al.*, 2004; Trasatti *et al.*, 2011). Cattin *et al.* (1999) showed that neglecting the changes in Young's modulus between the top low-rigidity layers and the underlying half-space in shallow-dipping faults underestimates fault depth by 1 km and affects the estimated slip by only 8%. Neither of these uncertainties affects our interpretation of 2014 Mormori earthquake in this article.

The 2014 Mormori earthquake provides additional evidence for the nature of faulting for moderate-size earthquakes ($M_w \sim 6$) in this region, proposed to have occurred mainly within the sedimentary cover (Koyi *et al.*, 2000) and to be detached from the basement faulting at depth. Similar observations of surface shortening in the overlying sediments have been made for the recent earthquakes in the Zagros, including the 27 November 2005 (Nissen *et al.*, 2007; Amighpey *et al.*, 2014) and the 10 September 2008 (Nissen *et al.*, 2010; Faegh-Lashgary *et al.*, 2012) earthquakes in Qeshm and the 25 March 2006 Fin earthquake (Roustaei *et al.*, 2010). The previously unmapped blind-thrust fault that was activated in the 2014 Mormori event dies out upward into the Gachsaran salt (Fig. 3c), which acts as a viscous or incompetent unit, causing stress diffusion; no reports of clear surface rupture have yet been reported for this earthquake, nor is there any phase discontinuity observed in the InSAR. Similar to the Gachsaran unit, the incompetent units within the Paleozoic sediment or Hormuz salt equivalent below the depths of 8–10 km strongly control and delimit any continuation of the faulting to depth (Fig. 3c).

CONCLUSIONS

We investigated source parameters and slip distribution for the 18 August 2014 M_w 6.2 Mormori earthquake in Iran using two pairs of ascending RADARSAT-2 interferograms. The InSAR analysis shows that the coseismic uplift affected the Dalpari anticline in the Dezful embayment of the Zagros; the anticline was uplifted by about 15 cm. The dislocation modeling and geological interpretation suggests that the faulting certainly occurred within the sedimentary cover, with the main slip restricted to depths between 3 and 10 km. This low-angle blind-thrust fault, dipping northeast, seems to be related to the local fold growth of the Dalpari anticline rather than blind basement faulting of the belt, providing evidence for seismogenic thin-skinned crustal shortening west of the Zagros mountain range.

ACKNOWLEDGMENTS

Original RADARSAT-2 data are copyright 2013–2014 MacDonald, Dettwiler and Associates Ltd (MDA). Part of this research was supported by the National Aeronautics and Space Administration's Earth Surface and Interior focus area and performed at the Jet Propulsion Laboratory, California Institute of Technology. We would like to thank Ziyadin Cakir, an anonymous reviewer and the Editor in Chief, Zhigang Peng, for their helpful comments on the original version of the manuscript. This study was supported by the Initiative and Networking Fund of the Helmholtz Association in the frame of Helmholtz Alliance "Remote Sensing and Earth System Dynamics."

REFERENCES

Amighpey, M., B. Voosoghi, and M. Motagh (2014). Deformation and fault parameters of the 2005 Qeshm earthquake in Iran revisited: A Bayesian simulated annealing approach applied to the inversion of space geodetic data, *Int. J. Appl. Earth Observ. Geoinform.* **26,** 184–192.

Amoruso, A., L. Crescentini, and C. Fidani (2004). Effects of crustal layering on source parameter inversion from coseismic geodetic data, *Geophys. J. Int.* **159,** no. 1, 353–364.

Atzori, S., and A. Antonioli (2011). Optimal fault resolution in geodetic inversion of coseismic data, *Geophys. J. Int.* **185,** no. 1, 529–538.

Atzori, S., I. Hunstad, M. Chini, S. Salvi, C. Tolomei, C. Bignami, S. Stramondo, E. Trasatti, A. Antonioli, and E. Boschi (2009). Finite fault inversion of DInSAR coseismic displacement of the 2009 L'Aquila earthquake (central Italy), *Geophys. Res. Lett.* **36,** no. 15, L15305, doi: 10.1029/2009GL039293.

Authemayou, C., O. Bellier, D. Chardon, L. Benedetti, Z. Malekzade, C. Claude, B. Angeletti, E. Shabanian, and M. R. Abbassi (2009).

Quaternary slip-rates of the Kazerun and the main recent faults: Active strike-slip partitioning in the Zagros fold-and-thrust belt, *Geophys. J. Int.* **178,** no. 1, 524–540.

Bahroudi, A., and H. Koyi (2003). Effect of spatial distribution of Hormuz salt on deformation style in the Zagros fold and thrust belt: An analogue modelling approach, *J. Geol. Soc.* **160,** no. 5, 719–733.

Berberian, M. (1995). Master "blind" thrust faults hidden under the Zagros folds: Active basement tectonics and surface morphotectonics, *Tectonophysics* **241,** nos. 3/4, 193–224.

Cattin, R., P. Briole, H. Lyon-Caen, P. Bernard, and P. Pinettes (1999). Effects of superficial layers on coseismic displacements for a dip-slip fault and geophysical implications, *Geophys. J. Int.* **137,** no. 1, 149–158.

Costantini, M. (1998). A novel phase unwrapping method based on network programming, *IEEE Trans. Geosci. Remote Sens.* **36,** no. 3, 813–821.

Faegh-Lashgary, P., M. Motagh, M. A. Sharifi, and M. A. Saradjian (2012). Source parameters of the September 10, 2008 Qeshm earthquake in Iran inferred from the Bayesain inversion of Envisat and ALOS InSAR observations, paper presented at *VII Hotine-Marussi Symposium on Mathematical Geodesy, International Association of Geodesy Symposia*, Rome, Italy, 6–10 June 2009, Springer-Verlag, Berlin, Germany, Vol. 137, 319–325, doi: 10.1007/978-3-642-22078-4.

Falcon, N. (1967). The geology of the north-east margin of the Arabian basement shield, *Advancem. Sci.* **24,** 1–12.

Fukuda, J. Ä., and K. M. Johnson (2008). A fully Bayesian inversion for spatial distribution of fault slip with objective smoothing, *Bull. Seismol. Soc. Am.* **98,** no. 3, 1128–1146.

Goldstein, R., and C. Werner (1998). Radar interferogram filtering for geophysical applications, *Geophys. Res. Lett.* **25,** 4035–4038.

Harris, R., and P. Segall (1987). Detection of a locked zone at depth on the Parkfield, California, segment of the San Andreas fault, *J. Geophys. Res.* **92,** 7945–7962.

Hessami, K., F. Jamali, and H. Tabassi (2003). *Major Active Faults of Iran, map*, International Institute of Earthquake Engineering and Seismology (IIEES), Tehran, Iran, scale: 1:2,500,000.

Hessami, K., F. Nilforoushan, and C. J. Talbot (2006). Active deformation within the Zagros Mountains deduced from GPS measurements, *J. Geol. Soc.* **163,** no. 1, 143–148.

Husseini, M. (1988). The Arabian infracambrian extensional system, *Tectonophysics* **148,** no. 1, 93–103.

Jackson, J. A. (1980a). Errors in focal depth determination and the depth of seismicity in Iran and Turkey, *Geophys. J. Int.* **61,** no. 2, 285–301.

Jackson, J. A. (1980b). Reactivation of basement faults and crustal shortening in orogenic belts, *Nature* **283,** no. 5745, 343–346.

Jackson, J. A., and T. Fitch (1981). Basement faulting and the focal depths of the larger earthquakes in the Zagros Mountains (Iran), *Geophys. J. Int.* **64,** no. 3, 561–586.

Konert, G., A. Afifi, S. Al-Hajri, K. De Groot, A. Al Naim, and H. Droste (2001). *Paleozoic Stratigraphy and Hydrocarbon Habitat of the Arabian Plate*, Chapter 24, American Association of Petroleum Geologists Memoir 74.

Koyi, H. A., K. Hessami, and A. Teixell (2000). Epicenter distribution and magnitude of earthquakes in fold-thrust belts: Insights from sandbox models, *Geophys. Res. Lett.* **27,** no. 2, 273–276.

Li, Z., J.-P. Muller, P. Cross, and E. J. Fielding (2005). Interferometric synthetic aperture radar (InSAR) atmospheric correction: GPS, moderate resolution imaging spectroradiometer (MODIS), and InSAR integration, *J. Geophys. Res.* **110,** doi: 10.1029/2004JB003446.

Maggi, A., J. Jackson, K. Priestley, and C. Baker (2000). A re-assessment of focal depth distributions in southern Iran, the Tien Shan and northern India: Do earthquakes really occur in the continental mantle? *Geophys. J. Int.* **143,** no. 3, 629–661.

Ni, J., and M. Barazangi (1986). Seismotectonics of the Zagros continental collision zone and a comparison with the Himalayas, *J. Geophys. Res.* **91,** no. B8, 8205–8218.

Nilforoushan, F., F. Masson, P. Vernant, C. Vigny, J. Martinod, M. Abbassi, H. Nankali, D. Hatzfeld, R. Bayer, F. Tavakoli, *et al.* (2003). GPS network monitors the Arabia–Eurasia collision deformation in Iran, *J. Geod.* **77,** nos. 7/8, 411–422.

Nissen, E., M. Ghorashi, J. Jackson, B. Parsons, and M. Talebian (2007). The 2005 Qeshm Island earthquake (Iran)—A link between buried reverse faulting and surface folding in the Zagros simply folded belt? *Geophys. J. Int.* **171,** no. 1, 326–338.

Nissen, E., F. Yamini-Fard, M. Tatar, A. Gholamzadeh, E. Bergman, J. R. Elliott, J. A. Jackson, and B. Parsons (2010). The vertical separation of mainshock rupture and microseismicity at Qeshm Island in the Zagros fold-and-thrust belt, Iran, *Earth Planet. Sci. Lett.* **296,** nos. 3/4, 181–194.

Okada, Y. (1985). Surface deformation due to shear and tensile faults in a half-space, *Bull. Seismol. Soc. Am.* **75,** 1135–1154.

Oveisi, B., J. Lavé, P. Van Der Beek, J. Carcaillet, L. Benedetti, and C. Aubourg (2009). Thick- and thin-skinned deformation rates in the central Zagros simple folded zone (Iran) indicated by displacement of geomorphic surfaces, *Geophys. J. Int.* **176,** no. 2, 627–654.

Roustaei, M., E. Nissen, M. Abbassi, A. Gholamzadeh, M. Ghorashi, M. Tatar, F. Yamini-Fard, E. Bergman, J. Jackson, and B. Parsons (2010). The 2006 March 25 Fin earthquakes (Iran)—Insights into the vertical extents of faulting in the Zagros simply folded belt, *Geophys. J. Int.* **181,** no. 3, 1275–1291.

Sahabi, F., and J. H. Macleod (1969). *Bala Rud geological map, scale 1:100,000*, Iranian oil Operating Company, Tehran, Iran.

Setudehnia, A., and J. T. OB-Perry (1967). *Dal Parri geological map, scale 1:100,000*, Iranian oil Operating Company, Tehran, Iran.

Sherkati, S., J. Letouzey, and D. Frizon de Lamotte (2006). Central Zagros fold-thrust belt (Iran): New insights from seismic data, field observation, and sandbox modeling, *Tectonics* **25,** no. 4, TC4007, doi: 10.1029/2004TC001766.

Tatar, M., D. Hatzfeld, and M. Ghafory-Ashtiany (2004). Tectonics of the central Zagros (Iran) deduced from microearthquake seismicity, *Geophys. J. Int.* **156,** no. 2, 255–266.

Trasatti, E., C. Kyriakopoulos, and M. Chini (2011). Finite element inversion of DInSAR data from the M_w 6.3 L'Aquila earthquake, 2009 (Italy), *Geophys. Res. Lett.* **38,** no. 8, L08306, doi: 10.1029/2011GL046714.

Vernant, Ph., F. Nilforoushan, D. Hatzfeld, M. R. Abbassi, C. Vigny, F. Masson, H. Nankali, J. Martinod, A. Ashtiani, R. Bayer, *et al.* (2004). Present-day crustal deformation and plate kinematics in the Middle East constrained by GPS measurements in Iran and northern Oman, *Geophys. J. Int.* **157,** no. 1, 381–398.

Walker, R., J. Jackson, and C. Baker (2003). Surface expression of thrust faulting in eastern Iran: Source parameters and surface deformation of the 1978 Tabas and 1968 Ferdows earthquake sequences, *Geophys. J. Int.* **152,** no. 3, 749–765.

Walker, R. T. (2006). A remote sensing study of active folding and faulting in southern Kerman province, SE Iran, *J. Struct. Geol.* **28,** no. 4, 654–668.

Walpersdorf, A., D. Hatzfeld, H. Nankali, F. Tavakoli, F. Nilforoushan, M. Tatar, P. Vernant, J. Chéry, and F. Masson (2006). Difference in the GPS deformation pattern of north and central Zagros (Iran), *Geophys. J. Int.* **167,** no. 3, 1077–1088.

Wang, L., S. Hainzl, M. Sinan Özeren, and Y. Ben-Zion (2010). Postseismic deformation induced by brittle rock damage of aftershocks, *J. Geophys. Res.* **115,** no. B10, B10422, doi: 10.1029/2010JB007532.

Wang, R., F. Diao, and A. Hoechner (2013). SDM—A geodetic inversion code incorporating with layered crust structure and curved fault geometry, in *EGU General Assembly 2013*, Vienna, Austria, 7–12 April 2013, Number EGU2013-2411.

Wang, R., F. L. Martín, and F. Roth (2003). Computation of deformation induced by earthquakes in a multi-layered elastic crust—FORTRAN programs EDGRN/EDCMP, *Comput. Geosci.* **29,** no. 2, 195–207.

Wegmuller, U., and C. Werner (1997). Gamma SAR processor and interferometry software, in *The 3rd ERS Symposium on Space at the Service of Our Environment*, Florence, Italy, 18–21 March 1997.

Wen, Y., C. Xu, Y. Liu, G. Jiang, and P. He (2013). Coseismic slip in the 2010 Yushu earthquake (China), constrained by wide-swath and strip-map InSAR, *Nat. Hazards Earth Syst. Sci.* **13,** 35–44, doi: 10.5194/nhess-13-35-2013.

Yamini-Fard, F., D. Hatzfeld, A. M. Farahbod, A. Paul, and M. Mokhtari (2007). The diffuse transition between the Zagros continental collision and the Makran oceanic subduction (Iran): Microearthquake seismicity and crustal structure, *Geophys. J. Int.* **170,** no. 1, 182–194.

Mahdi Motagh
Mahmud Haghshenas Haghighi
Hans-Ulrich Wetzel
GFZ German Research Center for Geosciences
Telegrafenberg Haus A17
14473 Potsdam, Germany
motagh@gfz-potsdam.de

Abbas Bahroudi
Exploration Department
School of Mining Engineering
Engineering Faculty
University of Tehran
515-14395 Tehran, Iran

Sergey Samsonov
Canada Centre for Mapping and Earth Observation
Natural Resources Canada
560 Rochester Street
Ottawa, Ontario
Canada K1A 0E4

Eric Fielding
Jet Propulsion Laboratory
California Institute of Technology
4800 Oak Grove Drive MS 300-233
Pasadena, California 91109 U.S.A.

Published Online 15 April 2015